IOSR Journal Of Applied Physics (IOSR-JAP)
e-ISSN: 2278-4861.Volume 15, Issue 3 Ser. I (May. – June. 2023), PP 01-09
www.Iosrjournals.Org

Influence Of Dopants Fe^{2+} And Yb^{3+} On Structural And Optical Properties Of $MnFe_2O_4$ Nanoparticles

Sudha Gulati
Department of Physics, Kalindi College, East Patel Nagar, New Delhi - 110008

Abstract
Co-precipitation is used to create cubic spinel manganese ferrite nanostructures that are both undoped and doped (Fe^{2+}, Yb^{3+}). X-ray diffraction (XRD), scanning electron microscopy (SEM), energy dispersive X-ray spectroscopy (EDX), and UV-visible absorption spectroscopy were used to examine the structural and optical characteristics of the nanoparticles. Through XRD patterns, a dopant's impact on microstructural parameters like size, cation radii, bond length, and lattice parameters is clearly visible. SEM images demonstrate the development of very dense nanocrystal formations and spherical shape. EDS spectra provide additional evidence of the nanoparticles' elemental composition. All findings show that the dopant has a major impact on the optical and microstructure of nanocrystals. The band gap of undoped $MnFe_2O_4$ is 1.2 eV, of Fe doped samples varies from 2.2 – 2.7 eV for x = 0.1 – 0.6, of Yb doped samples varies from 2.10 – 2.40 eV for x = 0.025 – 0.2.
Keywords : $MnFe_2O_4$; XRD; Band gap; bond length

Date of Submission: 21-04-2023 Date of Acceptance: 04-05-2023

I. Introduction

Cubic spinel structure can be represented by the general formula AB_2O_4, where divalent metal ions (A) occupy the tetrahedral sites (where A^{2+}= Ni^{2+}, Zn^{2+}, Mn^{2+} etc.) and trivalent metal ions (B) occupy octahedral sites (where B^{3+}= Fe^{3+}, La^{3+}, Al^{3+}, etc.)[1 - 3]. The scientific world has paid close attention to spinel ferrites, a significant class of magnetic materials that combine exceptional electrical, optical and magnetic properties. These materials are used in a wide variety of products, including switches, magnetic recorders, transformers, microwave devices, and computer memories, sensor [4 - 7]. Investigations into optical characteristics of these materials indicate that the properties are influenced by parameters during synthesis, doping element, preparation time, sintering temperature etc.[8 - 10]. Compared to other ferrites, manganese ferrite has a higher level of biocompatibility, making it more suitable for use in biomedical applications such drug delivery and magnetic resonance imaging (MRI)[11, 12]. A review of the literature reveals that a variety of physical and chemical methods, including ball milling, sol-gel, hydrothermal, auto combustion, thermal treatment, and the co-precipitation method, were used to synthesise pure and doped manganese ferrites[13 - 15].

According to literature survey, the optical band gaps depend on the size and composition of the materials. Thus, the band gap of the materials can be tailored for a particular application by altering either their composition or size[16, 17]. Amulthy et al used the microwave combustion method to create $Mn_{1-x}Co_xFe_2O_4$ (x = 0_0, 0.1, 0.2, 0.3, 0.4, and 0.5). The band gap of pure manganese ferrite was observed to be 1.76 eV and grew to 2.25 eV when the concentration of Co^{2+} ions increased[18]. Apostolova el al investigated effect Co, Mg and Ni doping on band gap of manganese ferrite and reported that band gap can increase or decrease using different ion doping [19]. By introducing a dopant, Bhalla et al. reported adjusting the band gap of Bi-doped nickel zinc (NiZn) spinel ferrite nanoparticles [20]. According to Devi et al., the optical band gap of nanoferrites $Mn_{1-x}Ni_xFe_2O_4$ (x=0.1, 0.2, 0.3, 0.4, and 0.5) is affected by Ni concentration, and a decrease in band gap was noted with an increase in Ni concentration [21]. Band gaps of 2.33 eV and 2.16 eV were found by Iranmahesh et al. for $MnFe_2O_4$ at pH values of 9 and 11, respectively[22]. According to Jose et al., the bandgaps for MnF (manganese ferrite), MnCoF, and MnCoMgF were 3.202 eV, 3.180 eV, and 3.239 eV, respectively[23]. The band gap of the sample shrinks when Co^{2+} is substituted in MnF, suggesting the quantum confinement phenomena. The band gap energy value rises when both Co^{2+} and Mg^{2+} were substituted.

There are no systematic reports on the optical properties of Fe^{2+} and Yb^{3+} doped manganese ferrite. In order to observe the effect on the band gap, Fe^{2+} and Yb^{3+} have been added to the manganese ferrite ($MnFe_2O_4$) system in the current work. The co-precipitation method is a useful technique for producing nanoparticles with a consistent composition in a short amount of time with a high yield. As a result, it was used to create the nanoparticles. No additional heat treatment is necessary for the procedure that is being provided. So, a straightforward low temperature chemical synthesis process was used to produce the Fe^{2+} and Yb^{3+} doped manganese ferrite nanoparticles. The preparation of Fe^{2+} and Yb^{3+} doped manganese ferrites nanoparticles

($MnFe_2O_4$) and examination of their structural, optical, and morphological characteristics utilising XRD, FESEM, EDX, and UV spectroscopy are the objectives of this work. Due to their high surface-to-volume ratio and controllable band gap, the produced magnetic nanoparticles may find use in photocatalysis, dye degradation, waste water treatment technology, etc.

II. Experimental

Material Synthesis

Fe^{2+} doped manganese ferrite nanoparticles

The $Mn_{1-x}Fe_xFe_2O_4$ (x=0.1, 0.2, 0.4 and 0.6) nanoparticles were prepared using reactants manganese chloride, ferric chloride and NaOH as the precipitating agent by the technique of co-precipitation. $MnCl_24H_2O$ solution (1M) and $FeCl_3.6H_2O$ solution (2M) were combined and ultrasonically mixed for five minutes. The boiling solution of NaOH was quickly added after the two solutions had been combined and heated to 60 °C. A black precipitate with a strong magnetic response was immediately formed. For two hours at 85°C, the solution was stirred with a magnetic device. The precipitate was then magnetically separated, several times washed with de-ionized water to remove any remaining electrolytes, and then washed with ethanol once the reaction mixture cooled to room temperature. The sample was vacuum-dried in the last phase, after which it was ground into a powder using a mortar and pestle to create nanoparticles. The samples are labelled as MF0, MF0.1, MF0.2, MF0.4, and MF0.6. The chemical reaction for the synthesis of nanoparticles $Mn_{1-x}Fe_x\ Fe_2O_4$:

$$(1\text{-}x)\ MnCl_2 + xFeCl_2 + 2FeCl_3 + 8NaOH \rightarrow Mn_{1-x}Fe_xFe_2O_4 + 8NaCl + 4H_2O$$

Yb^{3+} doped manganese ferrite nanoparticles

Using the co-precipitation technique, Yb-doped manganese ferrite nanoparticles were created. The measured amounts of $FeCl_3$ and $YbCl_3.H_2O$ were dissolved in deionized water to form 2M solution and the stoichiometric amount of $MnCl_2.4H_2O$ in deionized water (DI) was used to form 1.0M solution. The resultant solution (S1), obtained by mixing the above solutions, was heated to 60°C while being continuously stirred on a magnetic stirrer after being ultrasonically blended for 5 minutes at room temperature. In deionized water, a solution of NaOH was created (S2). This was heated before being combined with S1. Under magnetic stirring, the mixture was kept at 85°C for two hours. The final precipitate of synthesised nanoparticles was thoroughly washed in DI water multiple times before being rinsed with ethanol. The sample was vacuum-dried before being pulverised with a mortar and pestle to produce the $MnFe_{2-x}Yb_xO_4$ powder. $MnFe_{2-x}Yb_xO_4$ nanoparticles were produced using this process for x = 0.025, 0.075, 0.1, 0.15, and 0.2. The samples $MnFe_{2-x}Yb_xO_4$ (x = 0.025, 0.075, 0.1, 0.15, 1nd 0.2) are labelled as MFYb0.025, MFYb0.075, MFYb0.1, MFYb0.15, and MFYb0.2. The following reaction illustrates how $MnFe_{2-x}Yb_xO_4$ is created chemically:

$$MnCl_2 + (2-x)FeCl_3 + xYbCl_3 + 8NaOH \rightarrow MnFe_{2-x}Yb_xO_4 + 8\,NaCl + 4\,H_2O$$

Characterization

The powder XRD is captured using a Rigaku Ultima-IV X-ray diffractometer across a 2θ range of 20 to 80°. The crystal structure and phase purity of all the samples are investigated using a CuK_α with a wavelength of 1.5406 Å and a Ni filter to remove CuK_β. From XRD, microstructural parameters are also calculated. Using a Zeiss Gemini SEM500 equipped with energy-dispersive x-ray spectroscopy (EDS), the surface morphology, crystallite size, and microstructure of the materials were investigated. Using a Motras UV plus double beam UV-Vis spectrophotometer, absorption spectra between 200 and 900 nm were captured.

III. Results and Discussion

XRD studies

Fe^{2+} doped Manganese ferrite nanoparticles

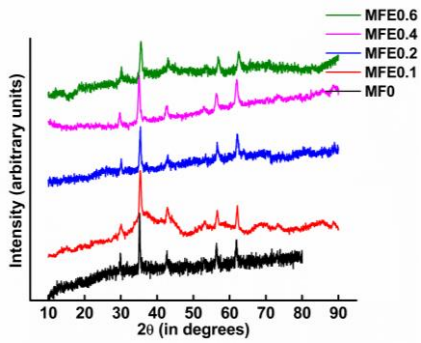

Figure 1 : X-ray diffraction (XRD) pattern of $MnFe_xFe_{2-x}O_4$ nanoparticles (where x = 0, 0.1, 0.2, 0.4, 0.6) : MF0, MFE0.1, MFE0.2, MFE0.4, and MFE0.4.

The structural characteristics of $Mn_{1-x}Fe_xFe_2O_4$ nanoparticles, such as phase, crystallite size, and various bond lengths, are calculated from XRD of the samples as shown in Figure 1. XRD pattern of as-prepared Fe^{2+} doped manganese ferrite nanoparticles amply demonstrates the existence of the pure ferrite phase. The peak was indexed to reflections (220), (311), (222), (400), (422), and (440), which supported the synthesis of a single-phase cubic spinel structure with space group Fd3m and absence of impurity phase, according to JCPDS Card No. 074-2403. As demonstrated in Fig. 1, the broadening of the (311) peak changes depending on the amount of Fe^{2+} dopant present in the sample. Full width at half maximum (FWHM) is determined by the fitting of the most intense diffraction peak (311) using the pseudo-Voigt peak shape function to the most intense diffraction peak (311) in order to estimate the crystallite size (D) of the nanoparticles using Debye-Scherrer's formula[24].

$$D = \frac{0.8\lambda}{\beta\cos(\theta)}$$

where λ is the wavelength of the X-ray wavelength used for diffraction, and β is the FWHM for the strongest peak at position (2θ). With more doping, the crystallite size shrinks. This might be because dopant Fe^{2+} has smaller ionic radii than dopant Mn^{2+}. Additionally, a change in the surface charge of nanoparticles may be the cause of this. The surface-to-volume ratio also varies due to the reduction in crystallite size, and this further alters the defect concentration. The hopping length, lattice parameter, and cation-oxygen bond length are all impacted by this shift in defect concentration. The various microstructural parameters can be calculated by taking into account the value of the oxygen positional parameter, u (~0.381), and the radii of oxygen ions, R_{O2-}= 1.29 Å.

The ionic radii at the tetrahedral site (R_A) and the octahedral site (R_B), hopping length at the tetrahedral site (L_A), hopping length at octahedral site (L_B), cation–oxygen ion bond lengths in tetrahedral site (d_{Ax}), cation–oxygen ion bond lengths in octahedral site (d_{Bx}), tetrahedral distance (d_{AxE}), octahedral shared distance (d_{BxE}), and unshared distances (d_{BxEU}) were calculated using the equations[25]

$$R_A = (u - 0.25)a\sqrt{3} - r_{O^{2-}}$$

$$R_B = (0.625 - u)a - r_{O^{2-}}$$

$$L_A = 0.25a\sqrt{3}$$

$$L_B = 0.25a\sqrt{2}$$

$$d_{Ax} = a\sqrt{3}\,(u - 0.25)$$

$$d_{Bx} = a\left[\sqrt{3u^2 - 2.75u + 0.671875}\right]$$

$$d_{AxE} = a\sqrt{4u - 1}$$

$$d_{BxE} = a\sqrt{2 - 4u}$$

$$d_{BxEU} = a\sqrt{4u^2 - 3u + 0.6875}$$

$$d_{Ax} = a\sqrt{3}\,(u - 0.25)$$

$$d_{Bx} = a\left[\sqrt{3u^2 - 2.75u + 0.671875}\right]$$

$$d_{AxE} = a\sqrt{4u - 1}$$

$$d_{BxE} = a\sqrt{2 - 4u}$$

$$d_{BxEU} = a\sqrt{4u^2 - 3u + 0.6875}$$

where a is the lattice parameter. Table 1 contains the calculated parameters. The table shows that all the parameters exhibit a reduction when the concentration of Fe^{2+} dopant increases. This Table further supports that Fe^{2+} dopant is successfully introduced into the lattice.

Table 1 Microstructural parameters obtained from XRD

sample	a (Å)	L_a (Å)	L_b (Å)	d_{Ax} (Å)	d_{Bx} (Å)	d_{AxE} (Å)	d_{BxE} (Å)	d_{BxEU} (Å)	Crystallite size nm
MFE0	8.462	3.664	2.992	1.920	2.066	6.125	5.838	2.993	29.8
MFE0.1	8.413	3.643	2.974	1.909	2.054	6.090	5.804	2.976	12.6
MFE0.2	8.391	3.633	2.967	1.904	2.049	6.074	5.789	2.968	20
MFE0.4	8.382	3.630	2.963	1.902	2.046	6.068	5.783	2.965	15.8
MFE0.6	8.365	3.622	2.957	1.898	2.042	6.055	5.771	2.959	10.9

Yb^{3+} doped Manganese ferrite nanoparticles

The face-centered cubic spinel structure of the synthesised Yb^{3+} doped nanoparticles with high crystallinity was revealed by XRD measurements[24]. The peaks of Bragg diffraction and the XRD pattern of JCPDS card number 74-2403 are in agreement with the Fd-3m space group. XRD peaks were seen for phases (220), (331), (400), (333), and (440)[24]. No peaks are present because of any additional impurities or any other secondary phases. Because there were no further phases in the current work, it can be concluded that Yb^{3+} ions are soluble in the host material and that the synthesis procedure was successful in incorporating Yb^{3+} ions into the manganese ferrite matrix despite the large differences in ionic radii of Mn^{2+} and Yb^{3+} ions. From the sharp and XRD peaks, it can be inferred that the samples have good crystallinity. All of the XRD patterns of the doped samples showed the peak shifting which further supports that the Yb^{3+} ions are incorporated in $MnFe_2O_2$.

Table 2: The values of crystallite size (cs), lattice parameter (a), and density (ρ) of $MnYb_xFe_{2-x}O_4$ nanoparticles

Sample	cs (in nm)	a (in Å)	P (in g/cc^3)
MF0	29.8	8.455	5.07
MFYb0.025	24.8	8.443	5.16
MFYb0.075	25.8	8.462	5.25
MFYb0.1	28.9	8.469	5.29
MFYb0.15	29.8	8.451	5.59
MFYb0.2	34.7	8.437	5.49

As ionic radius of Yb^{3+} is more than the ionic radius of Fe^{2+} ions, crystallite size of $MnFe_{2-x}Yb_xO_4$ nanoparticles is more than the crystallite size of $Mn_{1-x}Fe_xFe_2O_4$ nanoparticles (Table 2).

Though ionic radius of Yb^{3+} ion (0.86Å) is more than the ionic radius of the Fe^{3+} ion (0.63 Å), but it is observed that the substitution of Yb^{3+} ions result in the crystallite size (cs) in the range of 24 – 28.9 nm, which is smaller than cs of undoped sample, for lower values of dopant concentration x ($x \leq 0.1$). Such variations were also observed in the literature[25,26] The smaller cs can be attributed to differences in electronic configurations, valencies, and ionic radii between rare earth ions and Fe^{3+} ions [34]. The bond energy of Yb^{3+}-O^{2-} is greater as compared to that of Fe^{3+} - O^{2-}, thus an extra amount of energy is required to incorporate Yb^{3+} ions into $MnFe_2O_4$ to form Yb^{3+}-O^{2-} [27]. This extra energy hinders the process of crystallization and hence the growth of grains in $MnYb_xFe_{2-x}O_4$[28]. The substitution of Yb^{3+} ions in spinel structure also leads to iron vacancies and distorts the tetrahedral and octahedral symmetry, affecting crystallite size lattice parameters. Besides this, some Yb^{3+} ions may reside at the grain boundaries, which hinders grain growth and exerts pressure on the grain[29]. However, crystallite size for doped samples (for x = 0.15 and 0.2) is more than the undoped sample for higher values of x which could be attributed to the higher ionic radius of Yb^{3+} as compared to that for Fe^{3+}. In the present work, crystallite size is observed in the range 29.8nm – 34.7nm. Alonzian et al reported decrease in crystallite size (53.34nm – 28.77nm) with increase in concentration of dopant[30].

FESEM and EDS Studies

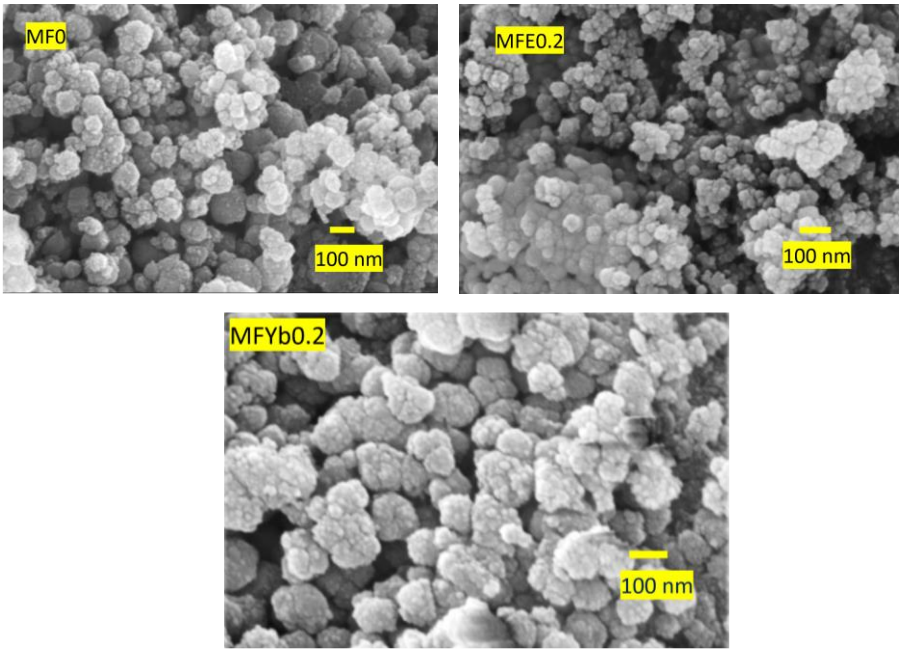

Figure 2 FE-SEM micrographs of (a) $MnFe_2O_4$ nanoparticles (MF0), (b) $Mn_{1-x}Fe_x$ Fe_2O_4 nanoparticles (MFE0.2), and (c) $MnYb_xFe_{2-x}O_4$ nanoparticles (MFYb0.2.

The morphologies of undoped $MnFe_2O_4$ nanoparticles (MF0), $Mn_{1-x}Fe_x$ Fe_2O_4 nanoparticles (x=0.2), and $MnFe_{2-x}Yb_xO_4$ nanoparticles (x=0.2), as representative sample, are depicted in FE-SEM micrographs in Figure 2. Sample MF0 sample had uneven flake-shaped nanoparticles, whereas samples that had been doped with Fe^{2+} and Yb^{3+} had isotropic spherical structures with homogenous uniform grain distribution. The average size of unsubstituted Mn ferrites is between 30 and 40 nm, whereas the average size of Fe^{2+} substituted $MnFe_2O_4$ nanoparticles is between 10 and 25 nm and Yb^{3+} doped manganese ferrite nanoparticles have the average size between 30 – 50 nm. Figure 4 displays the EDX spectra of undoped $MnFe_2O_4$ nanoparticles (MF0), $Mn_{1-x}Fe_x$ Fe_2O_4 nanoparticles (x=0.2), and $MnFe_{2-x}Yb_xO_4$ nanoparticles (x=0.2).

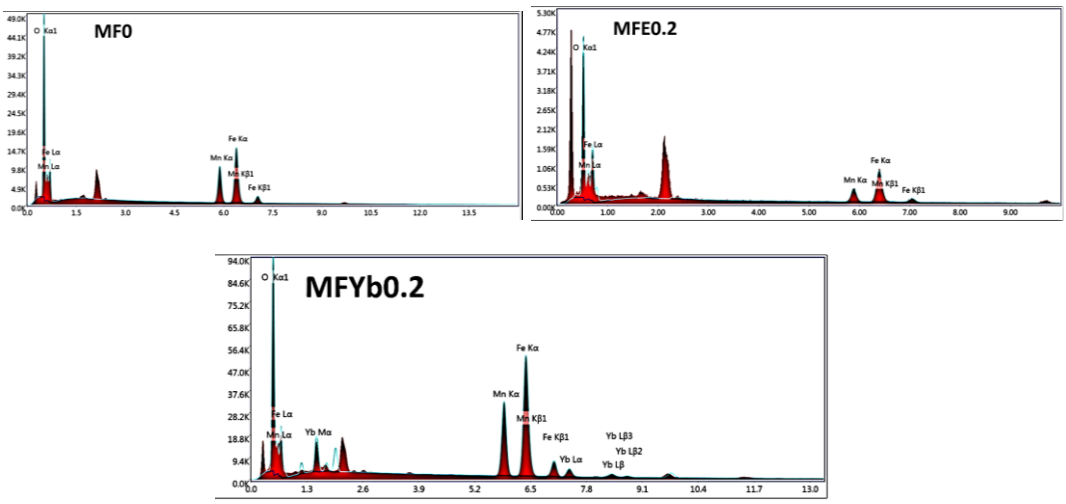

Figure 3 : EDX spectrum of (a) $MnFe_2O_4$ nanoparticles (MF0), (b) $Mn_{1-x}Fe_x$ Fe_2O_4 nanoparticles (MFE0.2), and (c) $MnYb_xFe_{2-x}O_4$ nanoparticles (MFYb0.2.

The samples included all the elements, including iron, oxygen, and manganese, according to the EDX spectrum. There were no signs of contaminants or other substances. Iron to oxygen (Fe:O) and metal ion composition ratios (Mn:Fe) / Mn:(Fe+Yb) were found to be consistent with the predicted composition ratio[24]. This demonstrates that the samples maintained the anticipated stoichiometry effectively. FESEM depicts agglomerated,

spherical-shaped nanoparticles. The EDS spectra of representative sample $MnFe_2O_4$, $MnFe_{2-x}Yb_xO_4$ (x = 0.2) indicate distinctive x-ray peaks of Mn, Fe and O atoms; and $MnFe_{2-x}Yb_xO_4$ indicates the distinctive x-ray peaks of Mn, Fe, Yb, and O atoms, but does not display peaks for any other element, proving the purity of the samples.

UV-Vis Spectroscopy Studies

According to Tauc equation, the manganese ferrite nanoparticles' direct band gap (E_g) is related to photon energy (hv)[31]

$$(\alpha\, h\nu)^2 = C\,(h\nu - E_g)$$

where α is the absorption coefficient, h is Planck's constant, C is a constant of proportionality, E_g is the optical band gap of the material, and ν is the frequency of radiation. The absorption coefficient α was determined from the absorption data using the following equation

$$\alpha = 2.303\ (\frac{A}{t})$$

where A is the absorption and t is the thickness of the sample.

By extrapolating the linear section of the curve (Tauc plots of$(\alpha h\nu)^2$ as a function of photon energy (hν), to $\alpha h\nu$ = 0, it is possible to calculate the.band gap can be determined by extrapolating the linear region of the curve (Tauc plots of $(\alpha h\nu)^2$ as a function of photon energy $h\nu$) to $\alpha h\nu$ = 0.

Tauc plots of $(\alpha h\nu)^2$ as a function of photon energy $h\nu$ is shown in Figure (4) for all the $Mn_{1-x}Fe_x$ Fe_2O_4 nanoparticles. The straight portion of the curve is extrapolated to determine the band gap.

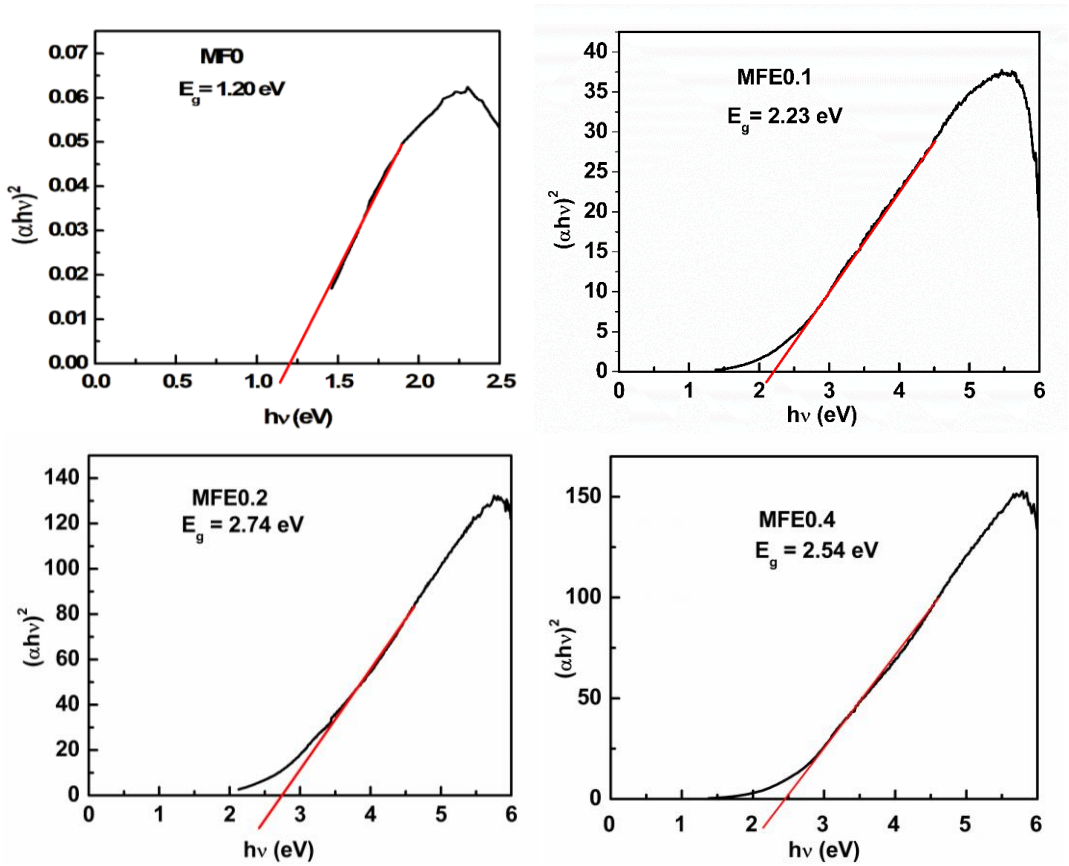

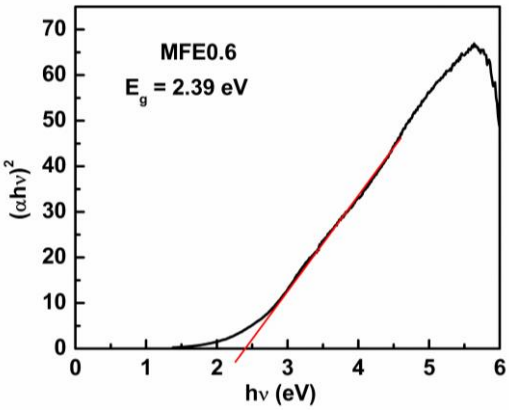

Figure 4 : Tauc plots of $Mn_{1-x}Fe_x$ Fe_2O_4 nanoparticles : MF0, MFE0.1, MFE0.2, MFE0.4, and MFE0.6

The band gap of the samples fluctuates with doping and ranges from 1.20 eV to 2.74 eV, as seen in Figure 4. In the literature, such band gaps have been recorded[32,21]. The band gap is found to be at its maximum for the sample with x=0.2. Figure 5 and Table 1 show that the band gap variation with doping can be associated with crystallite size variation. The quantum size effects can be used to explain an increase in band gap with a decrease in crystallite size when doping concentration varies from x= 0 to 0.2. The decrease in the band gap with an decrease in the crystallite size of the nanoparticles (for x=0.4, and 0.6) is attributed to surface and interface effects[31, 22].

The band gap for doped $MnFe_{2-x}Yb_xO_4$ nanoparticles falls in the range of 2.1 – 2.4 eV as shown in figure 5. Thus the band gap of doped samples is more than the band gap of undoped samples. The band gap increases with increase in x. The band gap varies inversely with crystallite size for the doped samples having $x \leq 0.1$. However, band gap varies directly with crystallite size for the doped samples having x = 0.15 and 0.2. An increase in the band gap with a decrease in size of the nanoparticles is attributed to the quantum size effect and an increase in the band gap with an increase in the size of the nanoparticles is attributed to surface and interface effects.

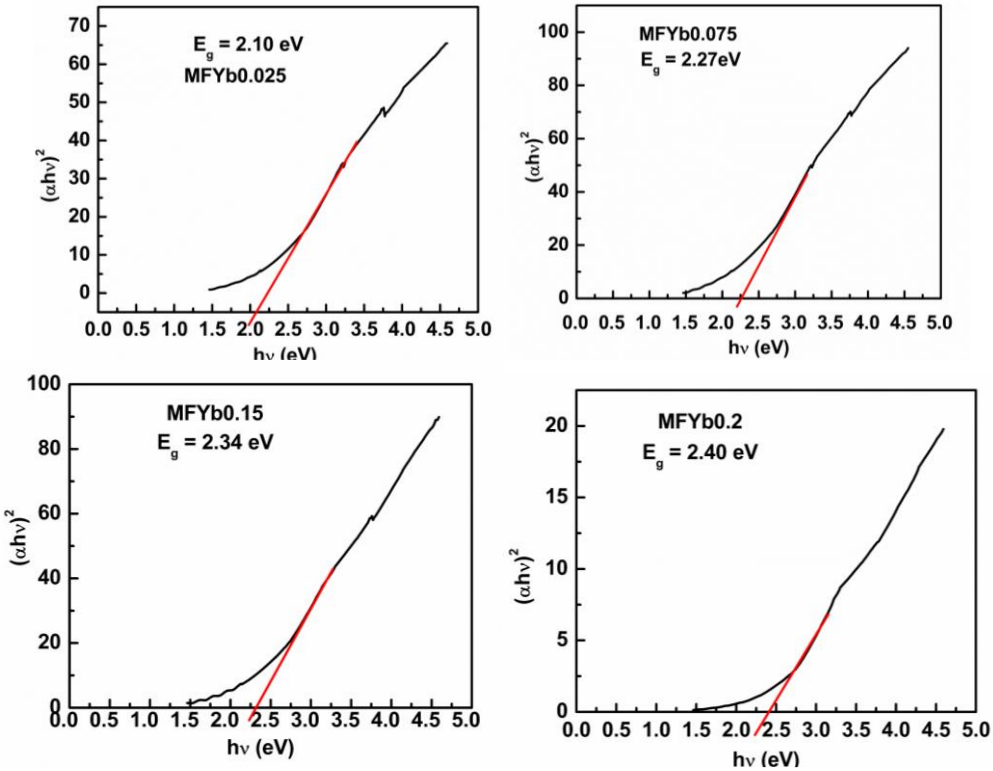

Figure 5 : Tauc plots of $MnFe_{2-x}Yb_xO_4$ nanoparticles : MFYb0.025, MFYbE0.075, MFYb0.15, and MFYb0.2

The band gap of Fe doped samples is higher than Yb^{3+} doped samples. Although there is a correlation between E_g with cs, E_g is dependent on multiple factors like crystallinity, synthesis method, process parameters, etc., hence it is difficult to quantify the trend.

It seems that additional sub-band-gap energy levels might be induced resulting in a smaller optical band gap when x>0.2 in Fe doped samples. However, band gap of Yb^{3+} doped samples increase with increase in x, though crystallite size increases. The increase in the band gap with an increase in the crystallite size of the nanoparticles is attributed to surface and interface effects The dopants can also be used to engineer band gaps for specific applications.

As photon energy of visible light ranges from 1.5 to 3 eV; Fe and Yb passes no threat to environment, thus doped manganese nanoparticles having a large surface-to-volume ratio with tuneable band gap can also be explored for applications in various fields such as solar cell technologies, opto-electronic devices, photovoltaic and photocatalytic degradation of pollutants.

IV Conclusions

Both undoped and doped (Fe^{2+}, Yb^{3+}) cubic spinel manganese ferrite nanostructures are produced by co-precipitation. As no additional heat treatment is required to produce nanoparticles, thus the Fe^{2+} and Yb^{3+} doped manganese ferrite nanoparticles were made using a simple low temperature chemical synthesis process. The structural and optical properties of the nanoparticles were investigated using X-ray diffraction (XRD), scanning electron microscopy (SEM), energy dispersive X-ray spectroscopy (EDX), and UV-visible absorption spectroscopy. A dopant's effect on microstructural factors like size, cation radii, bond length, and lattice parameters can be seen clearly by XRD patterns. FESEM photos show the growth of extremely dense nanocrystal formations and also their spherical form. EDS spectra offer additional proof of the elemental composition of the nanoparticles. The dopant significantly affects the optical and microstructure of nanocrystals, according to all available evidence. Undoped $MnFe_2O_4$ has a band gap of 1.2 eV, Fe^{2+} doped samples have band gap in the range of 2.2 to 2.7 eV for x = 0.1 to 0.6, and Yb^{3+} doped samples have a range of band gap 2.10 to 2.40 eV for x = 0.025 to 0.2.

References

[1]. Subramanian A P, Jaganathan S K, Manikandan A, Pandiaraj K N, N G and Supriyanto E 2016 Recent trends in nano-based drug delivery systems for efficient delivery of phytochemicals in chemotherapy RSC Adv. 6 48294–314

[2]. Almessiere M A, Slimani Y, Güngüneş H, Ali S, Manikandan A, Ercan I, Baykal A and Trukhanov A V 2019 Magnetic Attributes of $NiFe_2O_4$ Nanoparticles: Influence of Dysprosium Ions (Dy^{3+}) Substitution Nanomaterials 9 820

[3]. Vellayappan M V, Jaganathan S K and Manikandan A 2016 Nanomaterials as a game changer in the management and treatment of diabetic foot ulcers RSC Adv. 6 114859–78

[4]. Douglas F J, MacLaren D A, Maclean N, Andreu I, Kettles F J, Tuna F, Berry C C, Castro M and Murrie M 2016 Gadolinium-doped magnetite nanoparticles from a single-source precursor RSC Adv. 6 74500–5

[5]. Wang W, Ding Z, Zhao X, Wu S, Li F, Yue M and Liu J P 2015 Microstructure and magnetic properties of MFe_2O_4 (M = Co, Ni, and Mn) ferrite nanocrystals prepared using colloid mill and hydrothermal method Journal of Applied Physics 117 17A328

[6]. Ott G, Wrba J and Lucke R 2003 Recent developments of Mn–Zn ferrites for high permeability applications Journal of Magnetism and Magnetic Materials 254–255 535–7

[7]. Agrafiotis C C and Zaspalis V T 2004 Self-propagating high-temperature synthesis of MnZn-ferrites for inductor applications Journal of Magnetism and Magnetic Materials 283 364–74

[8]. Hossain A, Sarker M S I, Khan M K R and Rahman M M 2020 Spin effect on electronic, magnetic and optical properties of spinel $CoFe_2O_4$: A DFT study Materials Science and Engineering: B 253 114496

[9]. Ramaprasad T, Jeevan Kumar R, Naresh U, Prakash M, Kothandan D and Chandra Babu Naidu K 2018 Effect of pH value on structural and magnetic properties of $CuFe_2O_4$ nanoparticles synthesized by low temperature hydrothermal technique Mater. Res. Express 5 095025

[10]. Ateia E E, El-Bassuony A A, Abdelatif G and Soliman F S 2017 Novelty characterization and enhancement of magnetic properties of Co and Cu nanoferrites J Mater Sci: Mater Electron 28 241–9

[11]. Hedayatnasab Z, Abnisa F and Daud W M A W 2017 Review on magnetic nanoparticles for magnetic nanofluid hyperthermia application Materials & Design 123 174–96

[12]. Chandunika R K, Vijayaraghavan R and Sahu N K 2020 Magnetic hyperthermia application of $MnFe_2O_4$ nanostructures processed through solvents with the varying boiling point Mater. Res. Express 7 064002

[13]. Aslibeiki B, Kameli P, Salamati H, Eshraghi M and Tahmasebi T 2010 Superspin glass state in $MnFe_2O_4$ nanoparticles Journal of Magnetism and Magnetic Materials 322 2929–34

[14]. Li J, Yuan H, Li G, Liu Y and Leng J 2010 Cation distribution dependence of magnetic properties of sol–gel prepared $MnFe_2O_4$ spinel ferrite nanoparticles Journal of Magnetism and Magnetic Materials 322 3396–400

[15]. Raghavender A T and Hong N H 2011 Dependence of Néel temperature on the particle size of $MnFe_2O_4$ Journal of Magnetism and Magnetic Materials 323 2145–7

[16]. Ghosh P K, Ahmed Sk F, Jana S and Chattopadhyay K K 2007 Photoluminescence and field emission properties of ZnS:Mn nanoparticles synthesized by rf-magnetron sputtering technique Optical Materials 29 1584–90

[17]. Manikandan A, Judith Vijaya J, Sundararajan M, Meganathan C, Kennedy L J and Bououdina M 2013 Optical and magnetic properties of Mg-doped $ZnFe_2O_4$ nanoparticles prepared by rapid microwave combustion method Superlattices and Microstructures 64 118–31

[18]. Amalthi P, Judith Vijaya J, John Kennedy L and Bououdina M 2016 Microwave Based Synthesis; Structural, Optical and Magnetic Measurements of Co^{2+} Doped $MnFe_2O_4$ j nanosci nanotechnol 16 715–22

[19]. Apostolova I N, Apostolov A T and Wesselinowa J M 2023 Magnetization, Band Gap and Specific Heat of Pure and Ion Doped $MnFe_2O_4$ Nanoparticles Magnetochemistry 9 76

[20]. Bhalla N, Taneja S, Thakur P, Sharma P K, Mariotti D, Maddi C, Ivanova O, Petrov D, Sukhachev A, Edelman I S and Thakur A 2021 Doping Independent Work Function and Stable Band Gap of Spinel Ferrites with Tunable Plasmonic and Magnetic Properties Nano Lett. 21 9780–8
[21]. Devi E C, Department of Physics, National Institute of Technology Manipur, Langol – 795004, Manipur, India, Soibam I, and Department of Physics, National Institute of Technology Manipur, Langol – 795004, Manipur, India 2017 A Low Temperature Synthesis and Optical Characterization of Mn-Ni Mixed Nanoferrites Indian Journal of Science and Technology 10 1–5
[22]. Iranmanesh P, Saeednia S, Mehran M and Dafeh S R 2017 Modified structural and magnetic properties of nanocrystalline $MnFe_2O_4$ by pH in capping agent free co-precipitation method Journal of Magnetism and Magnetic Materials 425 31–6
[23]. Jose D, Mildred S, Mary Sebastian R and Xavier S 2022 An Investigative Study on the effect of Dopants on Manganese Based Mixed Nano Ferrites Synthesized through Sol-Gel Method IOP Conf. Ser.: Mater. Sci. Eng. 1221 012036
[24]. Gulati S, Gokhale S and Luthra V 2023 Effects of Yb^{3+} Doping on Structural, Morphological, and Temperature Dependent Magnetic Properties of $MnFe_2O_4$ Nanoparticles J Supercond Nov Magn. https://doi.org/10.1007/s10948-023-06534-3.
[25]. Amri N, Massoudi J, Nouri K, Triki M, Dhahri E and Bessais L 2021 Influence of neodymium substitution on structural, magnetic and spectroscopic properties of Ni–Zn–Al nano-ferrites RSC Adv. 11 13256–68
[26]. Baig M M, Yousuf M A, Warsi M F, Agboola P O, Sher M and Shakir I 2019 Surfactant assisted synthesis of rare earth Dy^{3+} substituted $MnFe_2O_4$ nanoparticles Ceramics International 45 18014–22
[27]. Naik S R and Salker A V 2012 Change in the magnetostructural properties of rare earth doped cobalt ferrites relative to the magnetic anisotropy J. Mater. Chem. 22 2740–50
[28]. Ghone D M, Mathe V L, Patankar K K and Kaushik S D 2018 Microstructure, lattice strain, magnetic and magnetostriction properties of holmium substituted cobalt ferrites obtained by co-precipitation method Journal of Alloys and Compounds 739 52–61
[29]. Heiba Z K, Bakr Mohamed M, Arda L and Dogan N 2015 Cation distribution correlated with magnetic properties of nanocrystalline gadolinium substituted nickel ferrite Journal of Magnetism and Magnetic Materials 391 195–202
[30]. Alonizan N H and Qindeel R 2018 Structural and magnetic properties of ytterbium substituted spinel ferrites Appl. Phys. A 124 408
[31]. Kombaiah K, Vijaya J J, Kennedy L J, Bououdina M, Kaviyarasu K, Ramalingam R J, Al-Lohedan H A and Munusamy M A 2017 A Green approach: synthesis, characterization and opto-magnetic properties of $Mg_xMn_{1-x}Fe_2O_4$ spinel nanoparticles J Mater Sci: Mater Electron 28 10321–9
[32]. Mary Jacintha A, Manikandan A, Chinnaraj K, Arul Antony S and Neeraja P 2015 Comparative Studies of Spinel $MnFe_2O_4$ Nanostructures: Structural, Morphological, Optical, Magnetic and Catalytic Properties j nanosci nanotechnol 15 9732–40

Sudha Gulati. "Influence Of Dopants Fe^{2+} And Yb^{3+} On Structural And Optical Properties Of $MnFe_2O_4$ Nanoparticles." *IOSR Journal Of Applied Physics (IOSR-JAP)15(3),* 2023, pp. 01-09.